V European Conference on Computational Fluid Dynamics
ECCOMAS CFD 2010
J. C. F. Pereira and A. Sequeira (Eds)
Lisbon, Portugal, 14–17 June 2010

A MULTI-DIMENSIONAL SPATIAL SCHEME FOR MASSIVELY PARALLEL COMPRESSIBLE TURBULENT COMBUSTION SIMULATION

J. Bohbot[*], Q.H.Tran[*], A.Velghe[*], N.Gillet[*]

[*]Institut Français du Pétrole, IFP,

1-4 avenue de Bois-Préau, 92852 Rueil-Malmaison Cedex - France
e-mail: julien.bohbot@ifp.fr, Q-Huy.tran@ifp.fr, anthony.velghe@ifp.fr, nicolas.gillet@ifp.fr

Key words: Multidimensional scheme, combustion, parallel MPI solver, CFD

Abstract: *A Multidimensional scheme has been implemented in a massively parallel code and applied for turbulent combustion simulation. The scalar fluxes like mass, internal energy and turbulence quantities are computed using this new spatial scheme for the advection phase which drastically reduces the scalar diffusion in arbitrary grids for multi-dimensional flows. This non-linear finite-volume scheme is inspired from the two steps reconstruction philosophy of the anti-dissipative Vofire method but relies on a different procedure in the transversal step and a more appropriate min-max principle in the longitudinal step. This multi-dimensional scheme is tested on few basic advection test cases to assess the accuracy and the benefits on numerical results. In second part, direct injection Diesel engine calculation is performed to ensure the numerical robustness of the scheme for an industrial use. Moreover, this numerical scheme has been fully parallelized to reduce the calculation return time and we have also analysed speed-up performance on large super-scalar machine..*

1 INTRODUCTION

Understanding and developing new engine concepts requires more and more help from 3D CFD and combustion modelling. IFP have developed a parallel unstructured code devoted to internal CFD with spray and combustion modelling. This code named "IFP-C3D" is entirely dedicated to the simulation of compressible reactive flows with combustion and sprays. Moving-mesh strategies are integrated with all physical models needed to simulate internal combustion engines. The conservation equations have to be solved using the Arbitrary Lagrangian Eulerian formalism to take into account the effect of the moving geometric parts and of the large volume variation. IFP-C3D uses the

time-splitting method to split the physical time-step into three stages. The time-splitting begins with the source terms (stage A) , then follows a full implicit Lagrangian stage (stage B), and finally a sub-cycled explicit Eulerian phase (stage C). In Stage C, the vertices are moved from the Lagrangian trajectory calculated during Stage B to their final location calculated by the moving grid algorithm for the next time step. This translation needs the finite volume fluxes to be calculated. Originally, the fluxes of the scalar like mass, internal energy and turbulence quantities are computed between cells using a Quasi Second Order Upwind Scheme. The QSOU scheme is known as to be very dissipative in particular when the advection velocity is transverse to the cells. Combustion simulation are very sensitive to the dissipation that produces unphysical solutions. With a higher-order accurate reconstruction scheme, it is possible to capture complex flow structures with an adequate number of grid points, which is especially conspicuous for flows including vortex-like structure that appear in an internal combustion engine. Philosophies of most oscillation reducing methods are mainly based on one-dimensional convection equation, and it is often insufficient or almost impossible to be extended in multi dimensional flow situations. This problem is mainly attributed to the difficulty of defining monotonicity in multiple dimensions. While the TVD criterion provides the fundamental framework to ensure monotonicity in one dimension, it does not provide equivalent performance in multiple dimensions. The multidimensional scheme used here is based on the construction of anti-dissipative flux. The core of the method is the reconstruction at the interface between cells using discontinuous profiles in a cell. As in MUSCL scheme, the multidimensional scheme used here satisfies a local maximum principle that is more restrictive. This reconstruction procedure used in the multidimensional scheme is done to take into account the difference between longitudinal and transverse diffusion that has been clearly presented by Després [1]. Based on this multi-dimensional scheme named VOFIRE, a modification of the reconstruction procedure have been made to reduce oscillations at interfaces and to preserve the extrema values. This modified reconstruction procedure is named VOFIRE2 and it is this multidimensional scheme that is used in this paper.

2 IFP-C3D DESCRIPTION

IFP-C3D code is fully parallelized for shared and distributed memory computer and uses optimised parallel mathematical libraries for linear algebraic system calculations. The conservation equations are solved using the Arbitrary Lagrangian Eulerian method to take into account the effect of the moving geometric parts and the large volume variation that occurs in internal combustion engine. IFP-C3D solves the conservation equations of mass, mass species, momentum energy and the k-ε turbulence equations for chemical reactive flows with sprays. Many fictive species are also used in the code to model tracers of real species or to add tracers for physical modelling. Fictive species satisfied the conservation equation of mass and momentum but are not taken into account for conservation of energy. IFP-C3D uses the time-splitting method to split the physical time-step into three stages. The time-splitting begins with the source terms (stage A), then follows a full implicit Lagrangian stage (stage B) and finally a sub-cycled explicit Eulerian phase (stage C). In Stage A, source terms of the chemical reactions on gas (auto-ignition, combustion, post-oxydation, chemical equilibrium...) of

the Lagrangian fuel injection (spray, liquid film) and of the spark ignition (AKTIM model [7], ISSIM model) are calculated and added to the conservation equations.

In the second stage, Stage B (Lagrangian stage), the original Semi-Implicit method introduced by Patankar [9] is retained in its fully implicit version. The coupled implicit equations (momentum, temperature and pressure) are solved with the SIMPLE algorithm. The SIMPLE method consists of an iteration on the coupled equations until the maximum number of iterations is reached or if the convergence criterion on the initial pressure is reached. The pressure equation is solved using the BiCGSTAB iterative method with ILU preconditioning. The temperature and velocity equations are solved using the residual conjugate gradient with Jacobi preconditioning. When the SIMPLE algorithm has converged, the diffusion terms of the turbulent equation are solved. The use of the ILU preconditioning and of the BiCGSTAB method for the pressure solver gives a better rate of convergence of the SIMPLE algorithm to avoid small pressure oscillations. The use of the conjugate residual method to solve the pressure equation was not able to reach the severe convergence criterion for the pressure without excessive consumption of time. If we note r_k the residual and b the second member, the criterion of the convergence in IFP-C3D is set to $\|r_k\|^2 < \varepsilon_P.\|b\|^2$ with ε_P a constant. If the convergence criterion is set to ε_P equal to 1.e-20, the CPU time needed to solve the pressure equation becomes excessively high with the Conjugate Residual method whereas the ILU/BiCGSTAB spent the same time for all the convergence criteria. These timings were obtained for a Port Fuel Injection engine calculation. Moreover, the ILU(0) preconditionning and the BiCGSTAB iterative method associated to the high convergence criterion increased the robustness of the Stage B algorithm for all diffusion solvers (temperature, velocity).

In Stage C, the vertices are moved from the Lagrangian trajectory calculated during Stage B to their final location calculated by the moving grid algorithm for the next time step. This translation needs the finite volume fluxes to be calculated. The fluxes of the scalar like mass, internal energy and turbulence quantities are computed between cells using a Quasi Second Order Upwind Scheme. Using connectivity of cells/face, slopes are calculated with the Superbee limiter. The faces of the control volume surrounding the vertex are also moving and the momentum fluxing calculates fluxes of momentum through each facet of the vertex. The slopes for the momentum fluxes are computed with the Van Leer limiter. The computed slopes allow the calculation of scalar values at the center of faces and vector values at the middle of the edge. These slope calculations ensure a second-order upwind advection for every scalar and momentum.

One of the key issues in the 3D simulation of combustion chambers is the mesh movement strategy due to moving boundaries (e.g. intake / exhaust valves, piston). This strategy is usually not acceptable for grid-based numerical methods because of the risk of extremely distorted meshes. Consequently, remeshing techniques are needed to ensure good mesh quality over the entire engine cycle. Generally, a remapping algorithm is used for Arbitrary Lagrangian Eulerian (ALE) simulations to ensure the coherence between the motion of the computational grid and the motion of the fluid. These remapping algorithms need fixed grid connectivity and cannot be used for global remeshing. The remapping techniques developed in IFP-C3D ensure global remeshing including a varying grid connectivity.

Because the grid resolution is generally low near the walls, a turbulent wall law and a heat transfer law should be used. Kays and Crawford law (Angelberger *et al.* [4]) is available in IFP-C3D. Kinetic energy dissipation and heat transfer are directly integrated in the turbulence and internal energy equations. Velocities are corrected and projected on the wall under slip conditions. These projections used in phase B and C are made knowing each orthogonal vector to each face. Three kinds of nodes on the wall are defined. For free nodes no projection is made. For nodes near a geometrical acute corner, a projection should be made following the corner direction. For more general nodes, a projection should be made on a tangential plane at the wall. In order to solve intake and exhaust strokes for engines, open boundaries were implemented in IFP-C3D.

3 MULTIDIMENSIONNEL SCHEME VOFIRE 2

3.1 Multidimensional Scheme

3.1.1. Generic form

Let us consider the advection equation:

$$\partial_t c + u\partial_x c + v\partial_y c + w\partial_z c = 0\,, \tag{1}$$

where *c(t,x,y,z)* is the unknown scalar function, and *(u,v,w)* is the velocity which is assumed to be uniform for the moment. For convenience, we introduce the vector notations $\mathbf{x} = (x,y,z)$ and $\mathbf{u} = (u,v,w)$, so that equation (1) can be rewritten as

$$\partial_t c + \mathbf{u}\cdot\nabla c = 0\,, \tag{2}$$

where ∇ denotes the gradient with respect to the space variable **x**.

We wish to compute an approximation for the solution of (1) over the discretized **x**-domain

$$\mathrm{R}^3 = \bigcup_{k\in Z} \overline{T_k}\,, \tag{3}$$

where T_k is an open polyhedral cell. Its volume in R^3 is

$$V_k = \mu(T_k)\,, \tag{4}$$

where μ is the usual Lebesgue measure. For a fixed cell index *k*, we consider the neighbour cells of T_k and draw a distinction between *upwind* (or donor) cells *j* and *downwind* (or receiver) cells ℓ by writing

$$j \prec k \quad \text{if } \mathbf{u}\cdot\mathbf{N}_{k,j} \le 0\,,$$

$$\ell \succ k \quad \text{if } \mathbf{u}\cdot\mathbf{N}_{k,\ell} > 0\,.$$

As usual, $\mathbf{N}_{k,h}$ stands for the outward normal vector from T_k to T_h, whenever *h* is a neighbour of *k*. The norm of $\mathbf{N}_{k,h}$ is equal to the area of the common face $\overline{T_k} \cap \overline{T_h}$.

Let Δt be the time-step from time t^n to time t^{n+1}. To solve (2), we consider the general explicit scheme

$$V_k(\hat{c}_k - c_k) + \Delta t \sum_{\ell \succ k} (\mathbf{u}\cdot\mathbf{N}_{k,\ell})\, \overline{\overline{c}}_{k\to\ell} + \Delta t \sum_{j \prec k} (\mathbf{u}\cdot\mathbf{N}_{k,j})\, \overline{\overline{c}}_{j\to k} = 0\,. \tag{5}$$

To alleviate notations, we have omitted the superscript n in c_k and have used the hat instead of the superscript n+1 in $\hat{c}_k$. Before elaborating on why the flux symbols $\overline{\overline{c}}_{\cdot\to\cdot}$ are overlined twice, let us mention that scheme (3) is typical of a finite-volume method. Indeed, it can be obtained by integrating the original equation (2) over the time-space control volume $]t^n, t^{n+1}[\times T_k$, by applying Green's theorem and by thinking of c_k and $\hat{c}_k$ as approximations of the cell averages

$$\hat{c}_k \approx \frac{1}{V_k}\int_{T_k} c(t^{n+1},\mathbf{x})d\mathbf{x} \qquad \text{and} \qquad c_k \approx \frac{1}{V_k}\int_{T_k} c(t^{n},\mathbf{x})d\mathbf{x}\,. \tag{6}$$

Introduce the non-negative dimensionless ratio

$$\nu_k = -\frac{\Delta t}{V_k}\sum_{j\prec k}\mathbf{u}\cdot\mathbf{N}_{k,j} = \frac{\Delta t}{V_k}\sum_{\ell\succ k}\mathbf{u}\cdot\mathbf{N}_{k,\ell}\,. \tag{7}$$

(the latter equality holds true because the sum of outward normal vectors over the faces of a cell always vanishes). For simplicity, we assume $\nu_k > 0$. This allows us to define the lighting coefficients

$$p_{kj} = \frac{\mathbf{u}\cdot\mathbf{N}_{k,j}}{\sum_{i\prec k}\mathbf{u}\cdot\mathbf{N}_{k,i}} \qquad \text{and} \qquad q_{k\ell} = \frac{\mathbf{u}\cdot\mathbf{N}_{k,\ell}}{\sum_{m\succ k}\mathbf{u}\cdot\mathbf{N}_{k,m}}\,. \tag{8}$$

It is straightforward to show that $p_{kj}\in[0,1]$, $q_{k\ell}\in[0,1]$, and moreover,

$$\sum_{j\prec k} p_{kj} = 1 \qquad \text{and} \qquad \sum_{\ell\succ \mathrm{k}} q_{k\ell} = 1. \tag{9}$$

Thanks to the above dimensionless parameters, scheme (5) becomes

$$\hat{c}_k = c_k - \nu_k\left\{\sum_{\ell\succ k} q_{k\ell}\,\overline{\overline{c}}_{k\to\ell} - \sum_{j\prec k} p_{kj}\,\overline{\overline{c}}_{j\to k}\right\}\,. \tag{10}$$

The schemes under the generic form (10) differ from each other by the flux values $\overline{\overline{c}}_{\cdot\to\cdot}$'s. Of this family, the first and most fundamental member is the standard upwind (or *donor*) scheme, which corresponds to

$$\overline{\overline{c}}_{j\to k} = c_j \qquad \text{and} \qquad \overline{\overline{c}}_{k\to\ell} = c_k\,, \tag{11}$$

and which can be transformed into

$$\hat{c}_k = (1-\nu_k)c_k + \nu_k\sum_{j\prec k} p_{kj}c_j\,. \tag{12}$$

From this, it is natural to define the averaged upwind value

$$c_k^{\bullet} = \sum_{j\prec k} p_{kj}c_j \tag{13}$$

and to observe that, as soon as $\nu_k\in[0,1]$, we have the cascading min-max principle

$$\hat{c}_k \in \left|c_k, c_k^{\bullet}\right| \qquad \text{and} \qquad c_k^{\bullet}\in\left|\{c_j\}_{j\prec k}\right|, \tag{14}$$

in which the symbol $|\ |$ designates the convex hull spanned by its arguments. But the donor scheme is notoriously known for its poor accuracy in the multi-dimensional

context. Our objective is to put forward an accuracy enhancement for the donor scheme based a two-sweep reconstruction process that reads

$$\overline{\overline{c}}_{j\to k} = c_j + \frac{1}{2}\delta c_{j\to k} + \frac{1-\nu_j}{2} Dc_{j\to k} \tag{15a}$$

$$\overline{\overline{c}}_{k\to \ell} = c_k + \frac{1}{2}\delta c_{k\to \ell} + \frac{1-\nu_k}{2} Dc_{k\to \ell} \tag{15b}$$

The correctors $\delta c_{\cdot\to\cdot}$ and $Dc_{\cdot\to\cdot}$ in (15) are respectively called *transverse* (or cross-wind) and longitudinal increments. These increments must be chosen so as to guarantee accuracy and stability for the scheme. The double line over the flux values $\overline{\overline{c}}_{\cdot\to\cdot}$ reflects the fact that this value is the outcome of a double reconstruction process.

3.1.2. Two-sweep reconstruction

The idea of a transverse corrector $\delta c_{\cdot\to\cdot}$ was first heuristically suggested by Després et al. [. Its purpose is to deal with cross-wind diffusion, while the classical longitudinal corrector $Dc_{\cdot\to\cdot}$. is meant to cope with diffusion in the direction of propagation. However, the formulae worked out by Després et al. [1] for the correctors do not seem to yield good results. This leads us to advocate a new approach to compute them.
Let *a*, *b* be two real numbers. We shall be using the notation

$$a \lhd b \tag{16}$$

to express that $b^- \le a \le b^+$, where $b^- = \min(b,0)$ and $b^+ = \max(b,0)$ are respectively the negative and positive parts of *b*. In other words, $a \lhd b$ means that *a* has the same sign as *b* but its absolute value is less than that of *b*.

The transverse corrector we are going to propose is significantly different from that of [1], even though it retains the basic idea. For each cell *k*, we first compute

$$A_k = \sum_{\ell\succ k} q_{k\ell}(c_\ell^\bullet - c_k)^+ \quad \text{and} \quad B_k = -\sum_{\ell\succ k} q_{k\ell}(c_\ell^\bullet - c_k)^- . \tag{17}$$

Then, we set

$$\delta c_{k\to\ell} = \Lambda\left(1, \frac{B_k}{A_k}\right)(c_\ell^\bullet - c_k)^+ + \Lambda\left(1, \frac{A_k}{B_k}\right)(c_\ell^\bullet - c_k)^- , \tag{18}$$

using any symmetric limiter function $\Lambda(.,.)$ subject to

$$\Lambda(\tau_L,\tau_R) \lhd 2\tau_L, \quad \Lambda(\tau_L,\tau_R) \lhd 2\tau_R, \quad \Lambda(\tau,\tau) = \tau . \tag{19}$$

The above constraints can be achieved, for instance, via the minmod, van Leer or superbee limiters [2]. It can be readily checked that this construction satisfies the outgoing flux constraint

$$\sum_{\ell\succ k} q_{k\ell}\delta c_{k\to\ell} = 0 , \tag{20}$$

which is necessary for stability analysis, as shown in [1].

Once the transverse step has been completed, we consider the partially reconstructed values

$$\bar{c}_{j\to k} = c_j + \frac{1}{2}\delta c_{j\to k}\,, \tag{21}$$

and let

$$\bar{c}_k^{\bullet} = \sum_{j\prec k} p_{kj}\bar{c}_{j\to k} = c_k^{\bullet} + \frac{1}{2}\sum_{j\prec k} p_{kj}\delta c_{j\to k} \tag{22}$$

be their mean value, computed using the same weights as those of the upwind value $c_k^{\bullet}$. We refer to $\bar{c}_k^{\bullet}$ as the *improved* upwind value. It can be shown that under the assumptions (19) for the limiter function, we are guaranteed that

$$\bar{c}_k^{\bullet} \in \left|\{c_j\}_{j\prec k}\right| \tag{23}$$

by the transverse reconstruction (17)-(18). In other words, the improved upwind value $\bar{c}_k^{\bullet}$ does not exceed the bounds (14b) already known for the initial upwind value $c_k^{\bullet}$.

We now proceed to determine the longitudinal correctors, which are also different from those of [1]. We propose to take

$$Dc_{k\to\ell} = \Lambda_k(c_k - \bar{c}_k^{\bullet}, c_\ell - \bar{c}_\ell^{\bullet})\,, \tag{24}$$

where Λ_k is any limiter function subject to

$$\Lambda_k(\sigma_L,\sigma_R) \lhd \frac{2}{\nu_k}\sigma_L, \quad \Lambda_k(\sigma_L,\sigma_R) \lhd \frac{2}{1-\nu_k}\sigma_R, \quad \Lambda_k(\sigma,\sigma) = \sigma\,. \tag{25}$$

Again, classical limiters such as minmod, van Leer, superbee are acceptable. The rationale for (25) is that it ensures

$$\hat{c}_k \in \left|c_k, \bar{c}_k^{\bullet}\right| \tag{26}$$

for $\nu_k \in [0,1]$. We are now in a position to state that the updated value $\hat{c}_k$ for the new scheme obeys a min-max principle (26)-(23) similar to (14) for the donor scheme.

The extension of this new scheme, called Vofire 2, to the case of a variable velocity field does not give rise to any specific difficulty. Therefore, we do not go into the details.

3.2 Numerical validation on 2D advection test case

3.2.1. Definition

In this numerical test we convect two chemical species (N_2 and O_2) through a three-dimensional mesh of hexahedral elements (100x100x3 elements) with a uniform velocity. The direction of the velocity has a great influence on the result. To improve the scheme properties the velocity is directed at a 45 degree angle to the mesh direction. This test case focuses on the transverse diffusion due to the fact that the velocity is not aligned with the mesh.

$$\begin{pmatrix} u \\ v \\ w \end{pmatrix} = \begin{pmatrix} 1 \\ 1 \\ 0 \end{pmatrix}$$

Equation 1 Initial Velocity

The dimensions of the simulated domain are equal to $l_x=5.10^{-2}$m, $l_y=5.10^{-2}$m and $l_z=1.5\ 10^{-3}$m. The convective CFL number used is equal to 0.7. A square function of mass fraction of N_2 is applied as initial condition which is transported by a uniform flow of O_2.The initial condition is plotted in Figure 1. The boundary conditions on the domain are periodic and we perform several cycles to follow the profile evolution.

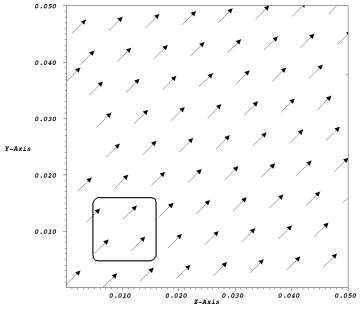

Figure 1 Initial Profile and velocity conditions

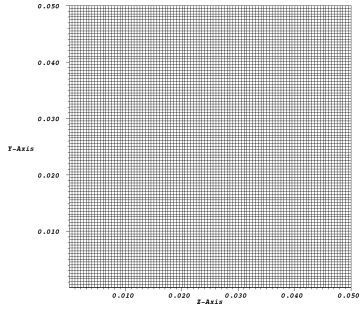

Figure 2 Mesh

3.2.2. Results

We compare the results of the quasi second-order upwind (QSOU) scheme and the VOFIRE scheme. The first results consist of advection with the QSOU scheme and the results are displayed for two times (t=0.1s and t=0.2s) in Figure 3. Figure 3 (b) represents the N_2 mass fraction iso-line after two cycles.
The transverse diffusion is significant and the initial profile (Figure 3 (a)) spreads in the transverse direction. We can see the iso-lines after four cycles in the Figure 3 (c). The square profile is not preserved but the propagation keeps the symmetry structure.

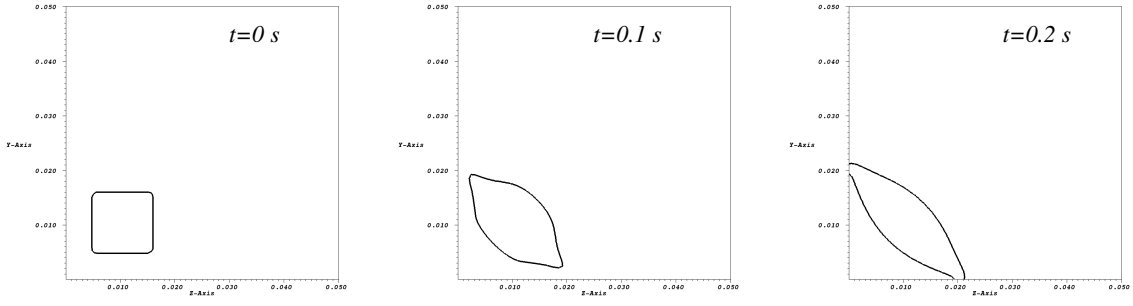

(a) Initial condition (b) After Two cycles (c) After Four cycles

Figure 3 N_2 mass fraction transported by QSOU scheme

The following results (Figure 4) represent a 2D slice of the O_2 mass fraction in the velocity direction at different times. The maximum and minimum of O_2 mass fraction are computed. We can observe that the minimum mass fraction increases with the time. This result is in accordance with the spatial order of the scheme.

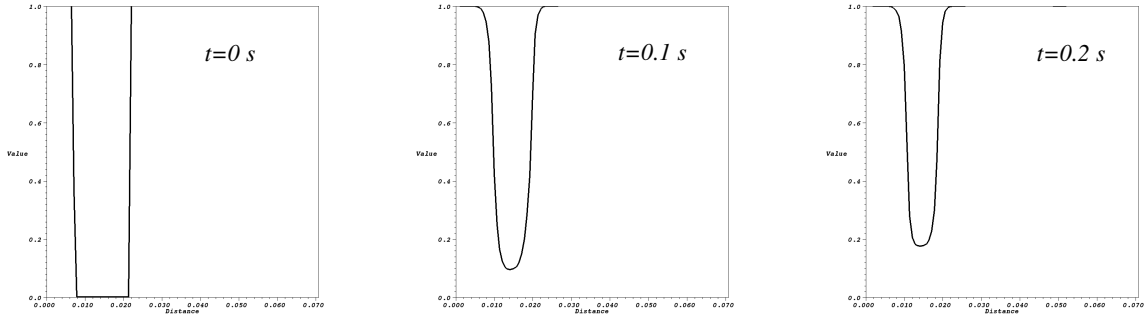

(a) Initial condition (b) Two cycles (c) Four cycles

Max=1.0 Min=0.0 Max=1.0 Min= 0.087 Max= 1.0 Min= 0.176

Figure 4 Slices of O_2 mass fraction profile

Now we perform the same numerical test with the VOFIRE scheme. The results (Figure 5) show the advection of the initial profile at two times (t=0.1s and t=0.2s) corresponding at two and four cycles. The iso-lines (Figure 5 (b) and (c)) shows that the global structure and the symmetry are preserved. The transverse diffusion is very well controlled by the VOFIRE scheme. We can observe a small deformation of the profile due to the transport of the species and the initial condition does not diffuse in the transverse direction like the QSOU scheme.

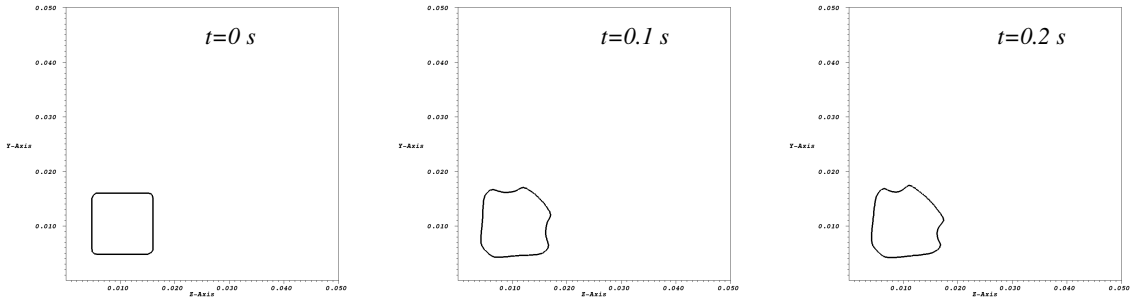

(a) Initial condition (b) Two cycles (c) Four cycles

Figure 5 N_2 mass fraction transported by VOFIRE scheme

Figure 6 represents a slice of the O_2 mass fraction profile at two times. The species are transported with constant extrema values.

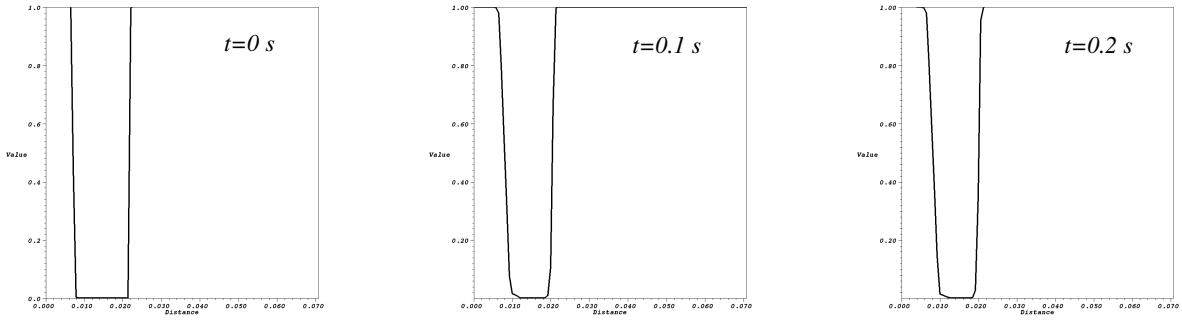

(a) Initial condition (b) After Two cycles (c) After Four cycles

Max=1.0 Min=0.0 Max=1.0 Min=0.0 Max=1.0 Min=0.0

Figure 6 Slices of O_2 mass fraction profile

The next results compare the QSOU and VOFIRE methods. The Figure 7 (a) and (b) shows the different O_2 mass fraction iso-lines and the slices of mass fraction profile compared with the initial condition after five cycles. The VOFIRE scheme shows a significant improvement on the transverse diffusion.

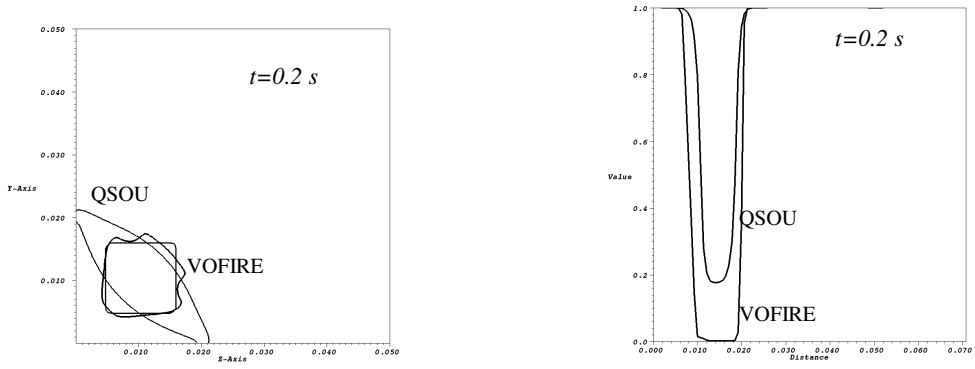

(a) Iso-lines of N_2 mass fraction (b) Slice of O_2 mass fraction profile

Figure 7 Comparisons QSOU/VOFIRE methods

3.3 Numerical validation on 3D advection test case

3.3.1. Definition

In this 3D numerical test, two chemical species (N2 and O2) through a three-dimensional mesh of hexahedral elements (100x100x100 hexas) is convected with a uniform velocity. To improve the scheme properties the velocity is directed at a 45 degree angle to the mesh direction. This test case focuses on the 3D transverse diffusion due to the fact that the velocity is not aligned with the mesh.

$$\begin{pmatrix} u \\ v \\ w \end{pmatrix} = \begin{pmatrix} 1 \\ 1 \\ 1 \end{pmatrix}$$

Equation 1 Initial Velocity

The dimensions of the simulated domain are equal to lx=5.10-2m, ly=5.10-2m and lz=5 10-2m. The convective CFL number used is equal to 0.7. A square function of mass fraction of N2 is applied as initial condition which is transported by a uniform flow of O2. The initial condition is plotted in Figure 8 and the mesh is shown in Figure 9. The boundary conditions on the domain are periodic.

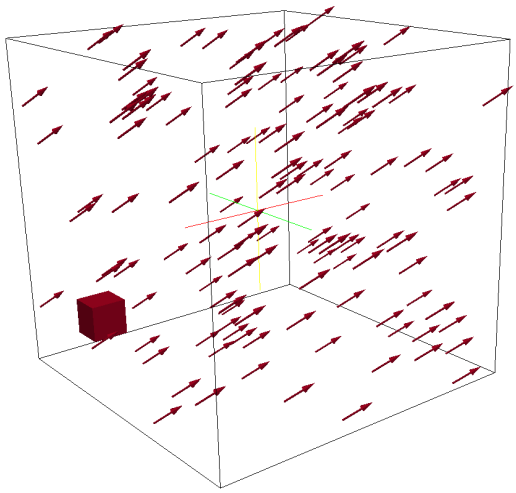

Figure 8: Initial Profile and velocity conditions

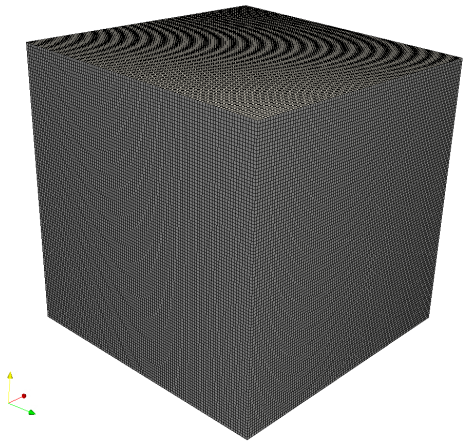

Figure 9: Grid used with 1Millions cells

3.3.2. Results

As in the 2D test case, we perform several cycles to follow the species mass evolution. In Figure 10 the iso_lines of the mass of 02 species is plotted in a plane for the simulation using the multidimensional scheme. The four pictures correspond respectively to the initial condition, first, second and third cycle. The iso-surface of 02 mass equal to 1 is also plotted to view the initial volume of mass. As it can be viewed, the iso-lines shows that the global structure and the symmetry are preserved as in the 2D case. The transverse diffusion is very well controlled by the multidimensional scheme. We can observe a small deformation of the profile due to the transport of the species and the initial condition does not diffuse in the transverse direction like the QSOU scheme. Moreover, the extreme value are constants with the VOFIRE scheme and we keep a sharp interface between O2 and N2.
Figure 11 presents the numerical results when using the QSOU advection scheme. The O2 mass is fully dispersed and the interface between O2 and N2 is diffused. Moreover, the extreme values are not conserved that can be problematic to describe accurately the liquid and gas fuel injection.

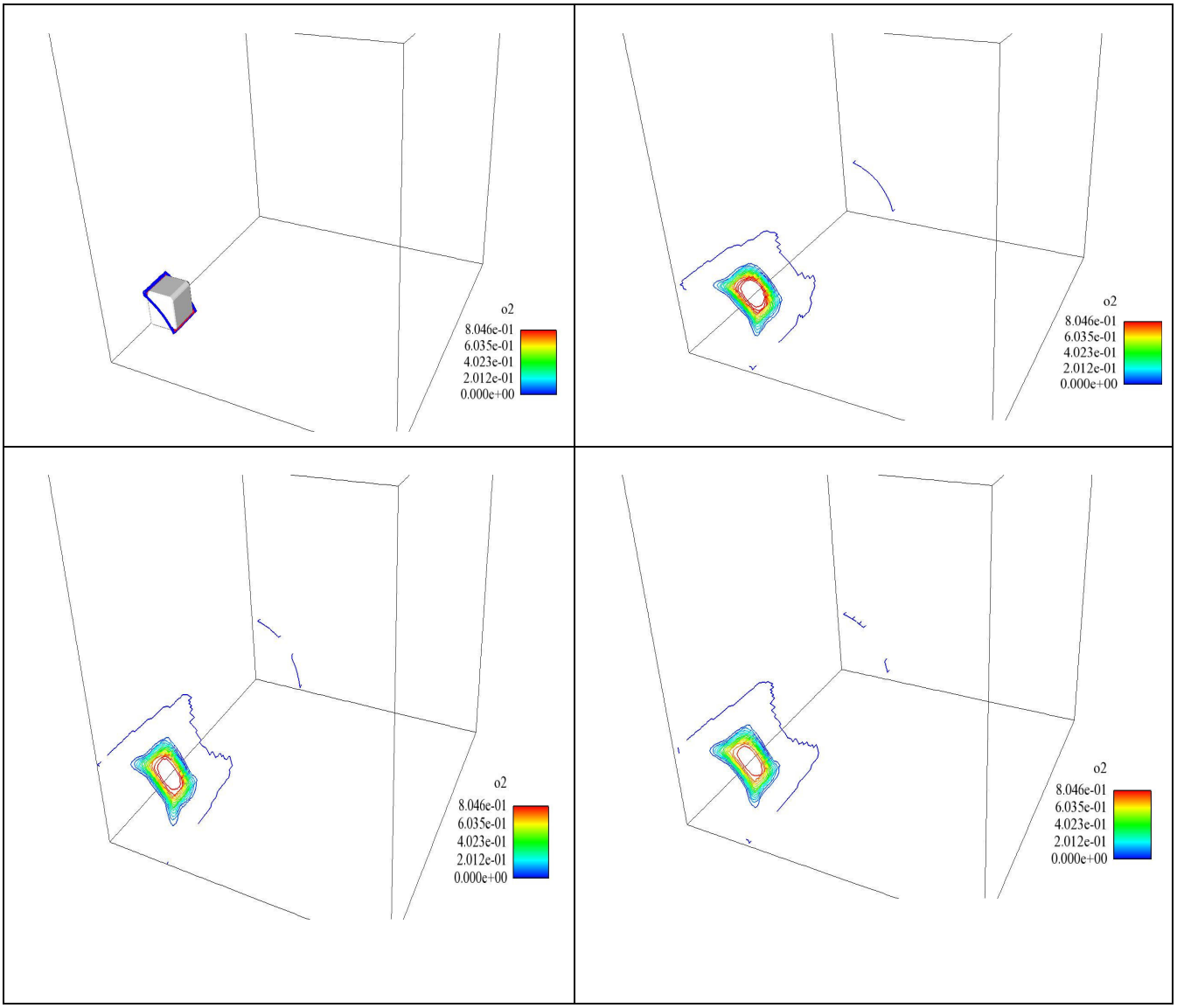

Figure 10: O2 mass iso-contour line obtained with VOFIRE scheme for 3 periods

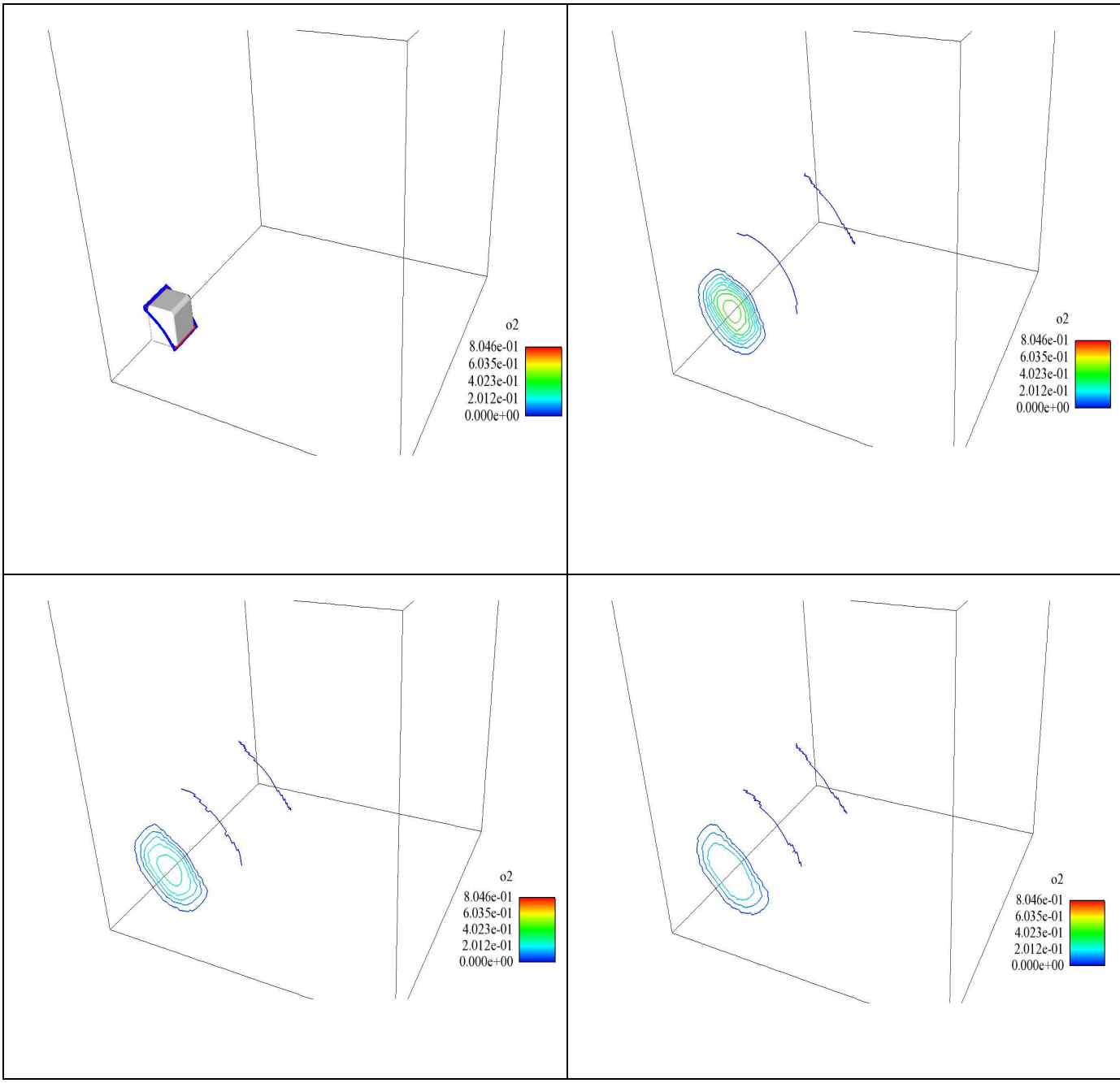

Figure 11: O2 mass iso-contour line obtained with QSOU scheme for 3 periods

3.3.3. Parallel and speedup performance results

To assess the industrial capability of the multidimensional scheme, a parallel performance analysis have been carried out to check the low CPU cost of the reconstruction procedure but also to assess the good behaviour of the scheme in a parallel purpose. Actually, the reconstruction procedure needs more MPI communication between domains to take into account the multidimensional reconstruction procedure for the calculation of the lighting coefficients. We have performed using from 8 processors to 128 processors the same 3D advection test case. The Figure 12 showed the partionning of the 1 millions cells on 64 processors. The

partitionning is performed with the METIS library fully integrated in the IFP-C3D code. All calculations has been performed on the IFP Cluster machine described in Table 1. This Cluster machine contains nodes containing quadri-core processors. Table 2 presents the calculation return time obtained for 3 periodic cycles for the QSOU and the VOFIRE2 scheme. As it can be viewed, the cost of the QSOU and the VOFIRE2 scheme is identical. The speed-up is identical when using the two different scheme. The speed-up is quite low between 8, 16 and 32 processors because of the too large number of cells per core. From 32 processors to 64 processors, the speed up is greater then the theory value of 2 thanks to the larger memory available when using 3 nodes.

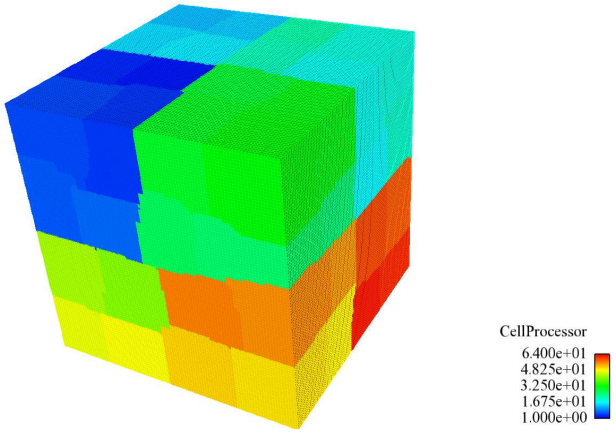

Figure 12: Mesh partitionning for 64 processors

IBM Cluster General Description	114 nodes Supermicro 1041M
Number of processors per node	4 processors AMD Barcelona
Processors characteristics	Quadri-core 2.3Ghz, 1Mo L2 memory
RAM per node	32Go DDR2 memory
Local disk capacity	160Go local disk
Interconnect network	Infiniband

Table 1: Cluster description

	8P	**16P**	**32P**	**64P**	**128P**
VOFIRE	9500s	7900s	5912s	2600s	1700s
	1	1.2	1.61	3,65	5,6
QSOU	9300s	7800s	5819s	2780s	1650s
	1	1.2	1.6	3.7	5.6
Cells per Processors	125.000	62.500	31.250	15.625	7.800

Number of nodes	1	1	2	3	4

Table 2: Performance and speed-up results

4 ENGINE SIMULATION

4.1 Diesel Direct Injection Engine

Homogeneous Charge Compression Ignition, or HCCI, is a relatively new combustion technology. It is a hybrid of the traditional spark ignition (SI) and the compression ignition process (such as a Diesel engine). Unlike a traditional S.I. or Diesel engine, HCCI combustion takes place spontaneously and homogeneously without flame propagation. This eliminates heterogeneous air/fuel mixture regions. HCCI is a *lean* combustion process. These conditions translate to a lower local flame temperature which lower the amount of Nitric Oxide (NOx) produced in the process. NOx is a gas that is believed to be responsible for the creation of ozone (O3). IFP-C3D is able to simulate this new combustion process thanks to the TKI (auto-ignition) and ECFM3Z combustion and the pollutant formation models. A HCCI engine is simulated with IFP-C3D using the VOFIRE and QSOU scheme with 16 processors that allow to reduce the calculation return time. The remapping method is used to reduce the number of cells during the compression phase and to add cells during the expansion phase. We used 6 different wedge meshes generated with the internal mesher to perform the calculations listed in Table 3.

Crank angle (deg.)	−140°	−77°	−51°	−35°	+36°	+52°	+80°
Number of cells in *Z*-direction	40	20	10	05	10	21	42
Number of cells	78000	45500	29250	21125	29250	47125	81250

Table 3

The main engine characteristics and the operating conditions are listed in . The injection is split into two injections at −7° and +11°. The EGR rate is equal to 53.5%. Raising the EGR level (up to 50%) has proven an effective way to control NOx emissions. It is proved that if combined with an appropriate injection strategy (the so-called “split injection strategy”) soot emissions can also be reduced. Simulations were performed using the up-to-date models on such running conditions. The simulation helped understand why a NADI™ combustion system did much better: the air entrainment, due to the vortex created by the first injection brings fresh air into the bowl beneficial for the second injection, giving it ideal mixing and burning conditions. Such an air entrainment is entirely due to the narrow spray cone angle combined with the specific piston shape. This phenomenon does not occur in a conventional combustion system where the second injection takes place in already rich or even burnt mixtures.
We have used the ECFM3Z combustion model (Colin et al [5]) and the TKI auto ignition model [6] to simulate the combustion phenomena. Figure 13 presents CO2

mass and spray visualisation for the calculation done with the two different scheme. As it can be viewed, the combustion phenomena behaviour is slightly different when using the multidimensional scheme. The combustion seems to be less diffusive than the QSOU scheme calculation. Figure 14 presents the in-cylinder pressure obtained with the two different scheme that assess the major effects of diffusion on combustion process. However, these two simulations demonstrate that the VOFIRE2 scheme has been successfully implemented in an industrial combustion code and can be used to perform complex industrial configuration simulations.

Bore (mm)	81
Stroke (mm)	88
Connecting rod length (mm)	160
Compression ratio	16:1
Engine speed (rpm)	1500
IMEP (bar)	5.7
EGR rate (%)	53.5
Fuel air equivalence ratio	0.904
Number of hole	6
Injected mass (mg)	15.3
SOI 1st injection	7 BTDC
SOI 2nd injection	13 ATDC
Second injection mass	3.915

Table 4:Engine operating conditions

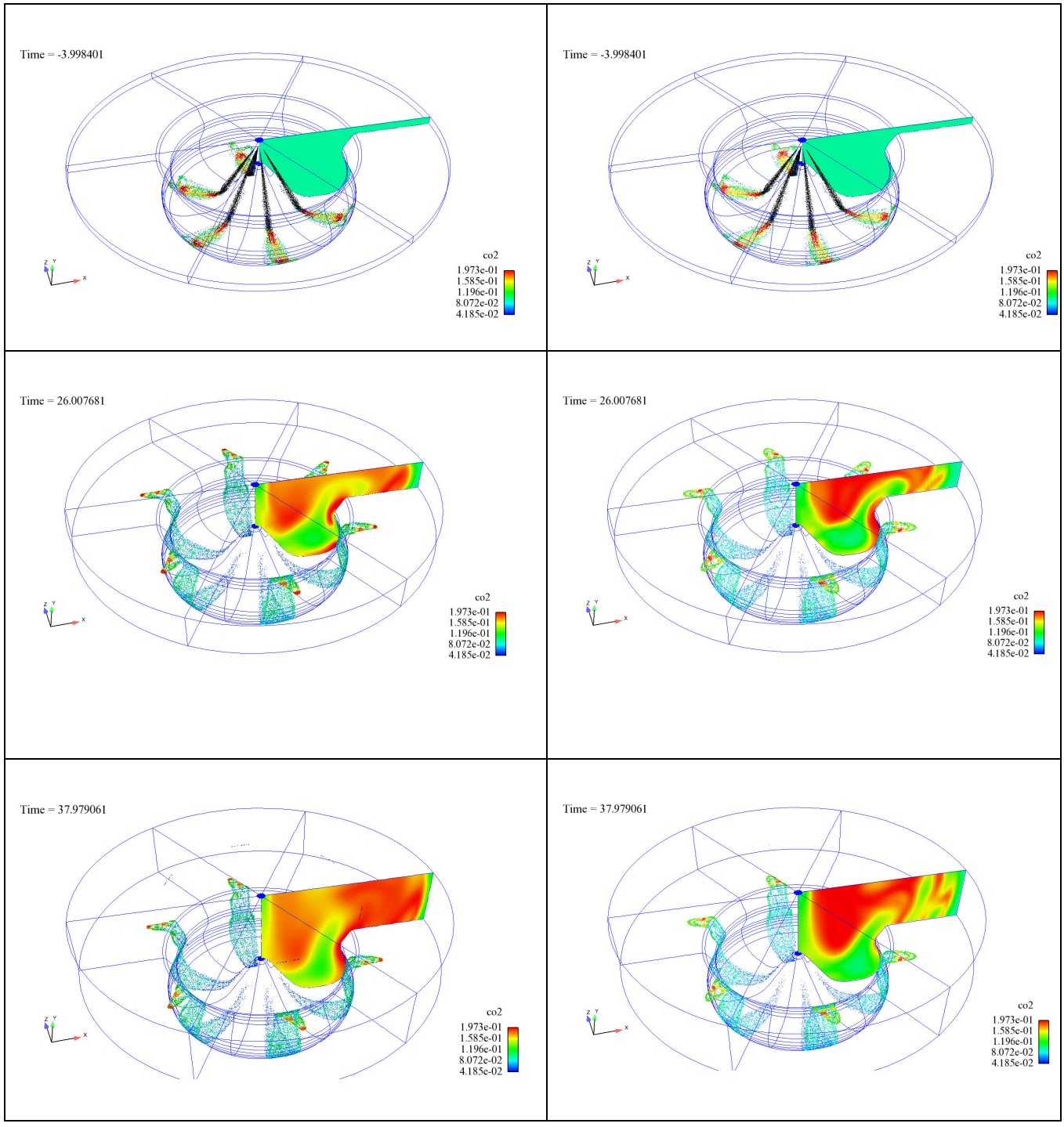

Figure 13: Combustion simulation with QSOU scheme (left) and VOFIRE scheme (right)

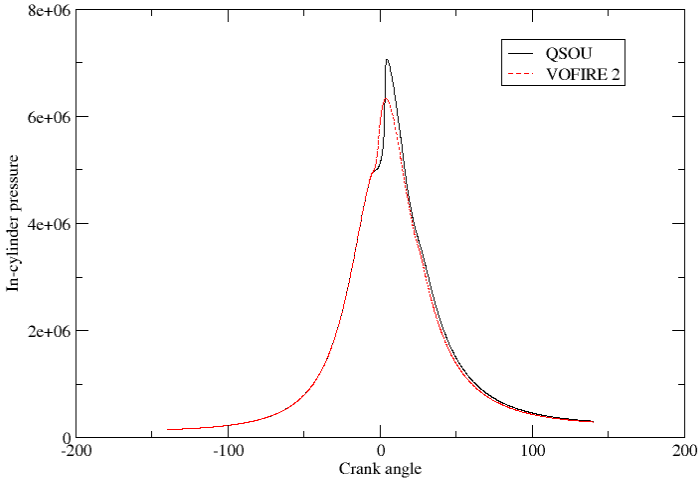

Figure 14: In-cylinder pressure

5 CONCLUSIONS

A robust and multi-dimensional scheme for compressible flows on unstructured grids is presented. Various numerical test cases clearly show the diffusion reduction obtained with the new reconstruction procedure. By maintaining the multi-dimensional monotonicity, numerical accuracy and robustness are significantly improved for linear and non-linear hyperbolic conservation law solver. The multidimensional scheme has been used to compute Diesel Direct Injection engine in a parallel purpose and it has been demonstrated that the multidimensional reconstruction procedure do not deteriorate CPU performance results and can be used to simulate complex industrial configurations. Next step will be to apply this multidimensional scheme to compute Eulerian liquid fuel injection in internal combustion engine using the Baer-Nunziato two-phase flow model.

REFERENCES

1. B. DESPRÉS, E. LABOURASSE, and F. LAGOUTIÈRE, *The Vofire method for multi-component flows on unstructured meshes*, Tech. Report R07052, Laboratoire Jacques-Louis Lions, 2007.
2. P. K. SWEBY, *High resolution schemes using flux limiters for hyperbolic conservation laws*, SIAM J. Numer. Anal., 21 (1984), pp. 995–1011.
3. "IFP-C3D: an Unstructured Parallel Solver for Reactive Compressible Gas Flow" J. Bohbot, N. Gillet, A. Benkenida, Oil Gas Sci. Tech., 64 (2009), 309-336
4. Angelberger, C., Poinsot, T., Delhaye, B., “Improving Near-Wall Combustion and Wall Heat Transfer Modeling in SI Engine Computations”, SAE paper 972881, 1997.
5. Colin O., Benkenida A., “The 3-Zones Extended Coherent Flame Model (ECFM3Z) for Computing Premixed Diffusion Combustion”, Oil & Gas Science and Technology, vol. 59, No 6, pp. 593-609, 2004.
6. Colin O., Pires da Cruz A. and Jay S., *Detailed chemistry-based auto-ignition model including low temperature phenomena applied to 3-D engine calculations*, Proceedings of the Combustion Institute, Vol. 30, pp. 2649-2656, 2005

7. Duclos J-M, Colin O., “Arc Kernel Tracking Ignition Model for 3D Spark-Ignition Engine Calculations”, paper (2-25), COMODIA 2001, 2001.
8. R.D. Reitz. Modeling atomization processes in high pressure vaporizing sprays. In *Atomization and Spray Technology*, volume 3, pages pp. 309-337, 1987
9. Patankar, S.V., Numerical Heat Transfer and Fluid Flow, Hemisphere Publishing Corp., Washington D.C., 1980.